Raman characterization of electronic transition energies of metallic single-wall carbon nanotubes

Hyungbin Son,[1] Alfonso Reina,[2] Ge. G. Samsonidze,[1] Riichiro Saito,[3] Ado Jorio,[4] Mildred S. Dresselhaus,[1,5] and Jing Kong[1,*]

[1]*Department of Electrical Engineering and Computer Science, MIT, Cambridge, Massachusetts 02139, USA*
[2]*Department of Material Science and Engineering, MIT, Cambridge, Massachusetts 02139, USA*
[3]*Department of Physics, Tohoku University and CREST, JST, Sendai 980-8578, Japan*
[4]*Departamento de Física, Universidade Federal de Minas Gerais, Belo Horizonte, MG 30123-970, Brazil*
[5]*Department of Physics, Massachusetts Institute of Technology, Cambridge, Massachusetts 02139, USA*

(Received 6 June 2006; published 18 August 2006)

Using a confocal micro-Raman system, spectra showing the splitting of optical transitions due to trigonal warping effect are presented for metallic single-wall carbon nanotubes (SWNT's). Our results indicate that the intensity variations between different optical transitions can be attributed primarily to the differences in the magnitude of the electron-phonon coupling matrix elements. Our approach will allow the study of the magnitude of electron-phonon matrix elements as well as quantum interference effects between different transitions in metallic SWNT's.

DOI: 10.1103/PhysRevB.74.073406 PACS number(s): 78.67.Ch, 73.22.−f, 78.30.Na, 78.66.Tr

Optical characterization methods such as photoluminescence excitation (PLE) and resonance Raman spectroscopy (RRS) provide powerful tools for characterizing the structures and studying important properties of single-wall carbon nanotubes (SWNT's), such as the optical transition energies and vibrational modes frequencies.[1,2] The optical transition energies E_{ii} obtained by these experimental studies have been successfully reproduced by using the extended tight-binding (ETB) method, including geometrical structure optimization,[3,4] and by further applying many-body (MB) logarithmic corrections[5] with empirical parameters.[6] Except for armchair nanotubes, two different optical transitions for metallic SWNT's are expected due to the trigonal warping effect, one with a lower transition energy $E^{\mathrm{M}}_{11\mathrm{L}}$ and a second with a higher transition energy $E^{\mathrm{M}}_{11\mathrm{H}}$.[7] Although many experimental data are available for $E^{\mathrm{M}}_{11\mathrm{L}}$ from previous Raman studies,[6,8] transitions associated with $E^{\mathrm{M}}_{11\mathrm{H}}$ were not observed in these Raman studies, and this has remained an open question. A recent work has reported $E^{\mathrm{M}}_{11\mathrm{H}}$ transitions using Rayleigh scattering and has attributed the lack of observations of $E^{\mathrm{M}}_{11\mathrm{H}}$ transitions in previous Raman experiments to different electron-phonon coupling strengths for $E^{\mathrm{M}}_{11\mathrm{L}}$ and $E^{\mathrm{M}}_{11\mathrm{H}}$ transitions.[9] However, no experimental evidence is given for the difference in electron-phonon coupling strengths for $E^{\mathrm{M}}_{11\mathrm{L}}$ and $E^{\mathrm{M}}_{11\mathrm{H}}$ transitions.

In this paper, we report the observation of $E^{\mathrm{M}}_{11\mathrm{H}}$ optical transitions for metallic nanotubes and show that the Raman signal intensity variations for the radial breathing mode (RBM) between different optical transitions provide a good match with the predictions of the ETB model, which includes excitonic effects and different coupling strengths for $E^{\mathrm{M}}_{11\mathrm{L}}$ and $E^{\mathrm{M}}_{11\mathrm{H}}$ transitions. The slight downshifts of the experimental transition energies for some observations are explained in terms of environmental effects.[10,11]

Figure 1 is the commonly used "Kataura plot," where the optical transition energies E_{ii} for different (n,m) structural indices are plotted against the RBM frequency (ω_{RBM}). The solid circles and squares (data points) are calculated by the ETB+MB model, where blue circles correspond to semiconducting SWNT's and red squares correspond to metallic SWNT's. These calculations match the experimental data for SDS-wrapped SWNT's very well.[3,6] The $2n+m$=const families are denoted by the solid lines and the $2n+m$ family numbers are also indicated on Fig. 1. Due to the trigonal warping effect, the family lines are split into two branches for each $2n+m$ metallic SWNT family.[3,7] The lower- and higher-energy branches correspond to the $E^{\mathrm{M}}_{11\mathrm{L}}$ and $E^{\mathrm{M}}_{11\mathrm{H}}$ transitions, respectively.[3]

Previous resonant Raman studies used the RBM signal and the optical transition energies associated with them to identify the (n,m) structural indices of SWNT's.[6] Recently, the electron-phonon matrix elements for RBM's were calculated by the ETB model, and it was shown that the electron-phonon coupling matrix elements for these unreported $E^{\mathrm{M}}_{11\mathrm{H}}$ transitions are weak [12] and that the quantum interference effects might also hinder the observation of $E^{\mathrm{M}}_{11\mathrm{H}}$ transitions.[13,14] Our present observations of such optical tran-

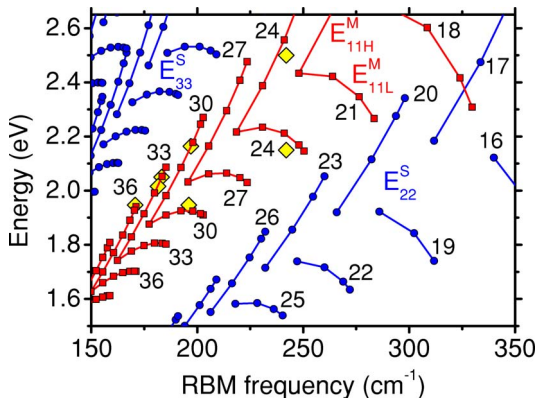

FIG. 1. (Color online) ETB+MB calculations of the optical transition energies versus ω_{RBM}. The blue circles and the red squares are semiconducting and metallic SWNT's, respectively. The $2n+m$=const families are denoted by solid lines and the $2n+m$ family numbers are also indicated. The yellow diamonds are experimental $E^{\mathrm{M}}_{11\mathrm{H}}$ and $E^{\mathrm{M}}_{11\mathrm{L}}$ optical transition energies.

sitions from individual metallic SWNT's confirm that the lack of their previous observation is due to the small magnitude of their electron-phonon matrix elements and show further that the experimental RBM intensities conform to predictions based on ETB theory.

Individual SWNT's are grown on a SiO_2 substrate by chemical vapor deposition (CVD) in methane at 900 °C using iron nanoparticles as the catalyst.[15] The as-grown SWNT's are analyzed with a confocal micro-Raman setup with a 50× objective (NA=0.8). The laser spot size is about 1 μm^2. Raman spectra are taken at 16 different laser excitation energies E_{laser} from 1.56 eV to 2.61 eV generated from an argon ion laser and a dye laser (R6G and DCM dye). At most of these 16 E_{laser} values, Raman spectra were taken over a 40 μm by 20 μm spatial area at a 0.5 μm by 1 μm spacing, resulting in 1701 spectra at each laser energy. A unique-shaped feature on the sample is used as a marker to identify the same spatial area at every laser excitation energies. As a result, about 150 SWNT's with diameters smaller than 1.5 nm were found in this spatial region, which ensures that the density of SWNT's is low enough, so that each Raman spectrum is essentially the spectrum of an individual SWNT or only a few SWNT's at most. This spatial mapping method allows us to follow and identify each nanotube, regarding its spatial position, and the method is particularly useful for recognizing when a particular SWNT goes in and out of resonance and for obtaining a resonance profile of each SWNT as a function of E_{laser}.[16,17] We do not find any influence of the iron nanoparticles to the Raman spectra of the SWNT. Since the repeatability of the microscope stage is better than 0.5 μm, the resolution of the spatial mapping (0.5 μm by 1 μm) determines the accuracy of the spatial position of nanotube. The RBM signals from the SWNT's are recorded simultaneously with the Raman signal from the Si, which is used for calibration. When the RBM signals at the same frequency appear at the same location at two different E_{laser} values, we conclude that the signals are coming from the same physical SWNT.[16] Figures 2(a) and 2(b) show such RBM signals at the same frequency (240 cm^{-1}) at the same location at two different E_{laser} (2.54 eV and 2.16 eV, respectively).

By varying E_{laser} and compiling the RBM intensities obtained at each different E_{laser}, we obtain an interesting two-peak resonance window for this SWNT [see Fig. 3(a)]. Since no semiconducting SWNT's with ω_{RBM}=240 cm^{-1} are resonant at any of the laser energies used, we determine that this is a metallic SWNT (see Fig. 1). The red circles represent the experimental integrated RBM intensity of this SWNT. The black curve shows the calculated resonance profiles for the integrated RBM intensity for both E^{M}_{11L} and E^{M}_{11H} transitions obtained from time-dependent third-order perturbation theory:

$$I(E_l) = C\left|\frac{m_{1L}M^{se}_{1L}M^{ep}_{1L}M^{la}_{1L}}{(E_l - E^{M}_{11L} - i\Gamma)(E_l - E_{ph} - E^{M}_{11L} - i\Gamma)} + \frac{m_{1H}M^{se}_{1H}M^{ep}_{1H}M^{la}_{1H}}{(E_l - E^{M}_{11H} - i\Gamma)(E_l - E_{ph} - E^{M}_{11H} - i\Gamma)}\right|^2, \quad (1)$$

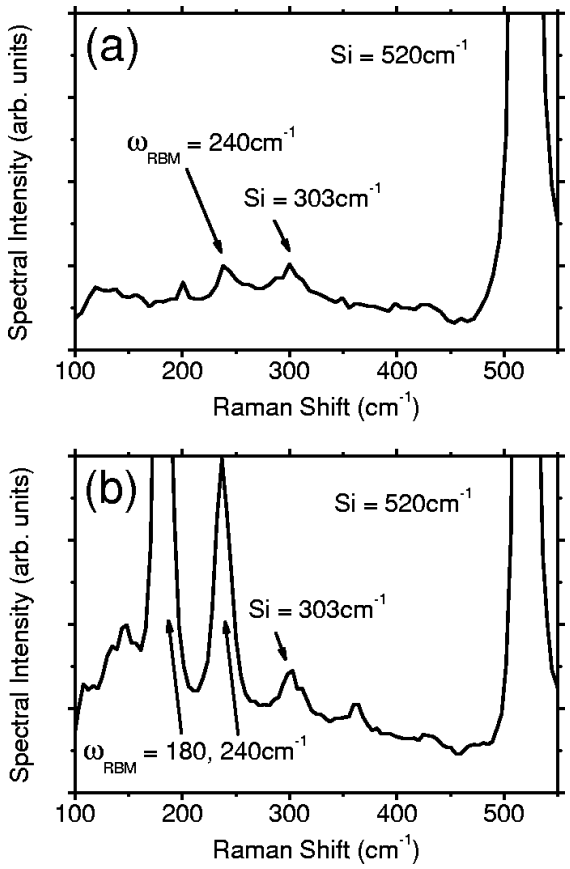

FIG. 2. RBM signals at the same spatial position at two different laser excitation energies (a) 2.54 eV and (b) 2.16 eV. The ω_{RBM}=240 cm^{-1} feature appears in both spectra.

where E_l is the laser excitation energy, M^{se}_{1X}, M^{ep}_{1X}, and M^{la}_{1X} (X=L,H) are the transition matrix elements for the spontaneous emission, electron-phonon scattering, and light absorption processes, respectively, E_{ph} is the RBM phonon energy, Γ is the broadening factor, and C includes all the other factors.[18] The effective masses m_{1L} and m_{1H} arise from the integration of the electron joint density of states, assuming that the transition matrix elements are independent of the wave vector in the range of reciprocal space contributing to the Raman intensity.[18] It should be noted here that optically excited states in SWNT's are excitonic in nature.[19,20] However, we restrict Eq. (1) to noninteracting excitations, since the exciton-photon and exciton-phonon transition matrix elements are not yet available in the literature. The interference between the E^{M}_{11L} and E^{M}_{11H} transitions is not considered since E^{M}_{11H}-$E^{M}_{11L}$is large compared to Γ and E_{ph} for the SWNT's we have investigated.

From the optical transition energy of the highest-intensity RBM peak and the RBM frequency, the SWNT in Figs. 2 and 3(a) is determined to be a (10,4) SWNT (see Fig. 1). ETB calculations for the (10,4) SWNT give the effective mass ratio m_{1L}/m_{1H}=0.46 (Ref. 21) and the matrix element ratios M^{la}_{1L}/M^{la}_{1H}=M^{se}_{1L}/M^{se}_{1H}=1.25 (Refs. 22 and 23) and M^{ep}_{1L}/M^{ep}_{1H}=3.75 (Ref. 12). We then find a ratio of 7.26 between the integrated intensities of the E^{M}_{11L} and E^{M}_{11H} peaks, as shown by the blue diamonds in Fig. 3(a). In order to fit the black curve from the above equation with our experimental

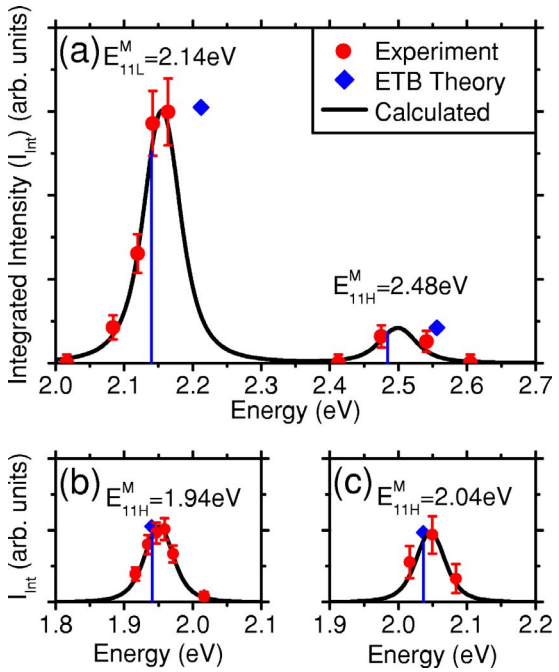

FIG. 3. (Color online) The resonance profile for (a) (10,4) SWNT, (b) (18,0) SWNT, and (c) (15,3) SWNT. The red circles are the experimental integrated RBM intensities. The SWNT intensities were calibrated against that of the 520-cm^{-1} Si peak. The blue diamonds are calculations using ETB+MB theory, and their horizontal positions correspond to the resonance energy. Regarding the intensity of the (10,4) SWNT, if we match the E^M_{11L} and E^M_{11H} results, we can then see that the experimental and theoretical results agree well (see text). The black line is the calculated RBM resonance profile using Eq. (1). The blue drop lines indicates the E^M_{11L} and E^M_{11H} values used for the calculated resonance profile. Note that the E^M_{11L} and E^M_{11H} differ from the peak center by $E_{ph}/2$ for the Stokes process. The experimental points are downshifted by 72 meV from the theoretical predictions for the (10,4) SWNT. All SWNT's show Γ=35 meV.

data points, one needs to adjust the broadening factor Γ and to make an overall downshift of both E^M_{11L} and E^M_{11H}. We can see that both the energy splitting between E^M_{11L} and E^M_{11H} (0.35 eV) and their integrated intensity ratio agree well between theory and experiment. There is, however, a downshift of 72 meV between the experimental results for both E^M_{11L} and E^M_{11H} when compared to the theoretical predictions. Since both E^M_{11L} and E^M_{11H} downshift by the same amount, we believe that the energy downshift is due to the different dielectric environment for our SWNT's as compared to SDS-wrapped SWNT's.[10,11] The presence of other SWNT's can cause an inhomogeneous dielectric environment even on the same substrate. The curve fitting gives rise to Γ=35 meV for all the three SWNT's shown in Fig. 3, which is also comparable to Γ values obtained in previous experiments.[6,24,25] The close match in the RBM intensity between the matrix element calculation and the experimental result indicates that the different intensities of the two resonances are due to differences in the matrix elements. Note that the ratio in the total optical matrix elements including the effective mass correction ($m_{1L}M^{la}_{1L}M^{se}_{1L}/m_{1H}M^{la}_{1H}M^{se}_{1H}$=0.72) is much closer to 1 than the ratio in the electron-phonon coupling matrix elements (M^{ep}_{1L}/M^{ep}_{1H}=3.75). Thus, the electron-phonon coupling matrix elements dominate the difference in the intensities for this particular case.

TABLE I. The comparison of E^M_{11L} and E^M_{11H} transition energies between theory and experiment for metallic SWNT's.

		ETB+MB Theory		Experiment	
n	m	E^M_{11L} (eV)	E^M_{11H} (eV)	E^M_{11L} (eV)	E^M_{11H} (eV)
10	4	2.21	2.56	2.14±0.02[a]	2.48±0.07[a]
13	4	1.92	2.18	1.95±0.07[b]	2.16±0.07[b]
15	3	1.81	2.05		2.04±0.02[a]
14	5	1.81	1.99		2.00±0.07[b]
18	0	1.70	1.94	1.655[c]	1.94±0.02[a]

[a]Full resonance profile is obtained for these transitions.
[b]These transitions are observed only at one excitation energy. The error is derived from the noise level and using the resonance profile with Γ=35 meV. The noise level is about 10% of the RBM signal intensity at the maximum of the resonance profile.
[c]Result from Ref. 24.

In Table I we list data for two other metallic SWNT's in addition to three metallic SWNT's shown in Fig. 3, for which we have observed the E^M_{11H} resonance. For the (10,4) and (13,4) nanotubes, we are able to detect the resonant Raman signal at both the E^M_{11L} and E^M_{11H} energies, whereas for the rest of the nanotubes, we were not able to examine the E^M_{11L} resonance due to the lack of a laser excitation source. However, their E^M_{11H} resonances are detected in our study, which has historically been much harder to see than the E^M_{11L} resonance signal. For the (10,4) nanotube, we have laser energies available to carry out the resonance profile determination as discussed above, but with the (13,4) nanotube, due to the unavailability of appropriate excitation sources, we are not able at present to obtain a resonant profile to compare with theory. As we can see from the table, the energies at E^M_{11H} match well with the ETB+MB calculations for all the data points, which are indicated by yellow diamonds in the Kataura plot in Fig. 1.

It was surprising to us that our ETB theory predictions based on noninteracting electrons and matrix elements that do not include excitonic effects explicitly can reproduce the experimental intensity so well for the (10,4) SWNT presented in this work. We are now accumulating more data to determine whether the match is accidental or whether it also applies to other SWNT's with different (n,m) indices or in different environments.

In summary, we present the observation of the optical transition corresponding to E^M_{11H} for metallic SWNT's. The integrated RBM intensities associated for the E^M_{11H} transitions are much lower than for E^M_{11L} transitions and the observed intensities conform to predictions of ETB theory. A good signal-to-noise ratio is required to observe the weak E^M_{11H} transitions. We achieved a strong enough signal in this work by taking the Raman spectrum of individual SWNT's with a high efficiency confocal micro Raman system. The observa-

tion of E_{11L}^{M} and E_{11H}^{M} transitions from the same SWNT further validates ETB theory. The experimental method presented in this work will allow an experimental determination of the magnitude of electron-phonon coupling matrix elements for individual SWNT's and of the quantum interference effects between E_{11L}^{M} and E_{11H}^{M} transitions that have been predicted for metallic SWNT's.[13,14]

MIT authors acknowledge support from NSF grant DMR04-05538 and Intel Higher Education Program. R.S. acknowledges support from NEXT grant (No. 16076201). A.J. acknowledges financial support from FAPEMIG and CNPq, Brazil. Work is carried out using the Raman facility in the Spectroscopy Laboratory supported by NSF-CHE 0111370 and NIH-RR02594 grants.

*Corresponding author. Email address: jingkong@mit.edu

[1] M. S. Dresselhaus, G. Dresselhaus, R. Saito, and A. Jorio, Phys. Rep. **409**, 47 (2005).
[2] S. M. Bachilo, M. S. Strano, C. Kittrell, R. H. Hauge, R. E. Smalley, and R. B. Weisman, Science **298**, 2361 (2002).
[3] Ge. G. Samsonidze, R. Saito, N. Kobayashi, A. Grüneis, J. Jiang, A. Jorio, S. G. Chou, G. Dresselhaus, and M. S. Dresselhaus, Appl. Phys. Lett. **85**, 5703 (2004).
[4] V. N. Popov, New J. Phys. **6**, 17 (2004).
[5] C. L. Kane and E. J. Mele, Phys. Rev. Lett. **93**, 197402 (2004).
[6] C. Fantini, A. Jorio, M. Souza, M. S. Strano, M. S. Dresselhaus, and M. A. Pimenta, Phys. Rev. Lett. **93**, 147406 (2004).
[7] R. Saito, G. Dresselhaus, and M. S. Dresselhaus, Phys. Rev. B **61**, 2981 (2000).
[8] J. Maultzsch, H. Telg, S. Reich, and C. Thomsen, Phys. Rev. B **72**, 205438 (2005).
[9] M. Y. Sfeir *et al.*, Science **312**, 554 (2006).
[10] M. J. O'Connell, S. Sivaram, and S. K. Doorn, Phys. Rev. B **69**, 235415 (2004).
[11] A. M. Rao, J. Chen, E. Richter, U. Schlecht, P. C. Eklund, R. C. Haddon, U. D. Venkateswaran, Y.-K. Kwon, and D. Tomanek, Phys. Rev. Lett. **86**, 3895 (2001).
[12] J. Jiang, R. Saito, Ge. G. Samsonidze, S. G. Chou, A. Jorio, G. Dresselhaus, and M. S. Dresselhaus, Phys. Rev. B **72**, 235408 (2005).
[13] A. G. Souza Filho, N. Kobayashi, J. Jiang, A. Grüneis, R. Saito, S. B. Cronin, J. Mendes Filho, Ge. G. Samsonidze, G. Dresselhaus, and M. S. Dresselhaus, Phys. Rev. Lett. **95**, 217403 (2005).
[14] J. Jiang, R. Saito, A. Grüneis, S. G. Chou, Ge. G. Samsonidze, A. Jorio, G. Dresselhaus, and M. S. Dresselhaus, Phys. Rev. B **71**, 205420 (2005).
[15] J. Kong, H. T. Soh, A. M. Casswell, C. F. Quate, and H. Dai, Nature (London) **395**, 878 (1998).
[16] Y. Yin *et al.* (unpublished).
[17] L. X. Zheng *et al.*, Nat. Mater. **3**, 673 (2004).
[18] R. M. Martin and L. M. Falicov, *Light Scattering in Solids I*, edited by M. Cardona, Topics in Applied Physics, Vol. 8 (Springer-Verlag, Berlin, 1983), pp. 79–145, Chap. 3.
[19] F. Wang, G. Dukovic, L. E. Brus, and T. F. Heinz, Science **308**, 838 (2005).
[20] J. Maultzsch, R. Pomraenke, S. Reich, E. Chang, D. Prezzi, A. Ruini, E. Molinari, M. S. Strano, C. Thomsen, and C. Lienau, Phys. Rev. B **72**, 241402(R) (2005).
[21] A. Jorio *et al.*, Phys. Rev. B **71**, 075401 (2005).
[22] A. Grüneis, R. Saito, Ge. G. Samsonidze, T. Kimura, M. A. Pimenta, A. Jorio, A. G. Souza Filho, G. Dresselhaus, and M. S. Dresselhaus, Phys. Rev. B **67**, 165402 (2003).
[23] We did not consider the dependence of the matrix elements on E_{laser} (Ref. 22) since our experimental data are calibrated at each E_{laser} using the Si peak intensity from the substrate.
[24] A. Jorio, A. G. Souza Filho, G. Dresselhaus, M. S. Dresselhaus, R. Saito, J. H. Hafner, C. M. Lieber, F. M. Matinaga, M. S. S. Dantas, and M. A. Pimenta, Phys. Rev. B **63**, 245416 (2001).
[25] S. B. Cronin *et al.*, Phys. Rev. Lett. **96**, 127403 (2006).